An Experimental Determination of the Kinetic Friction Coefficient of a Miniature Pool Table

John Schmidt
Department of Physics, The College of Wooster, Wooster, Ohio 44691, USA
(Dated: May 21, 2022)

The purpose of this experiment was to calculate the kinetic friction coefficient μ on a miniature pool table by analyzing the motion of a pool ball that travelled along and parallel to the miniature pool table's surface. By generating position versus time plots for the ball's motion, relevant data was extracted that allowed us to calculate $\mu = 0.288 \pm 0.002$. This value does meet the provided regulations for standard pool table cloth friction coefficients.

I. INTRODUCTION

The basic ideas responsible for the modern game of pool originated in 15th-century England. [1] Pool is typically categorized under the broader term of "billiards", which is commonly assumed to included any game that involves launching a series of balls into pockets within a table. The popularity of such billiards games has persisted throughout the ages, being both referenced in Shakespearean plays in the year 1600 and prominently featured in American movies in the latter half of the 20th century.

Pool is also of interest to a section of the scientific community, as gameplay requires application of many principles of physics. [6] Detailed understanding behind the science of pool is crucial to the development of corresponding assistive technology. [8] Such technology can help physically challenged individuals play the game, consequently providing improvements to their quality of life. With this potential application in mind, it is useful to conduct thorough research into any relevant aspects of pool game dynamics, as heightened understanding can help refine the development of assistive technology.

The purpose of this experiment is to find the friction coefficient μ of a miniature pool table, which is located in room 211 of Taylor Hall at the College of Wooster in Wooster, Ohio. Although friction itself may change between miniature and standard pool tables, the processes used to calculate μ could potentially be useful when analyzing other pool systems.

II. THEORY

Let B be the pool ball used for this experiment and T be the surface of the pool table on which B travels. Recall that the kinetic friction coefficient μ_k is used for friction acting on a sliding object. The static friction coefficient μ_s is used for friction acting on a non-moving or rolling (without sliding) object, which is usually much larger than μ_k. [5] In our case, we only consider our pool ball rolling without sliding. Therefore, we need to develop a theoretical model for the motion of B across T using the static friction coefficient μ_s.

For the purposes of simplifying our system, we make the following assumptions:

1. The form of B is a perfect sphere.
2. The mass m of B is uniformly distributed throughout B.
3. Both B and T are perfectly rigid.
4. The friction of the surface of B has negligible impact on the motion of B.
5. Friction is uniform throughout T.
6. The flatness of T makes T a horizontal plane that is orthogonal to the direction of gravitational acceleration g.
7. The motion of B forms a straight line parallel to T and can therefore be modelled in one dimension.

Assumptions 1 to 5 are justified in three ways. First, necessary system simplifications must be made in order to make due with available equipment, as alternative materials were unavailable. Second, due to time constraints, meaningful experimentation and calculation wouldn't have been able to take place without making these assumptions, as finding means to ensure ideal conditions was not feasible. Third, individual pool balls and tables are manufactured to be approximately the same, so any variance from these assumptions that may occur should be considered both inevitable and, because the effects on motion would affect each apparatus approximately equally, negligible. Assumptions 6 and 7 will be justified in the Section III of this report.

Regarding Assumption 4, it is noteworthy that prior studies regarding pool balls have resulted in an equation to determining the coefficient of kinetic friction (ball slides without rolling) μ_k of a standard pool ball/table system. [6] This value differs from the static friction coefficient (ball rolls without sliding) μ_s, which is primarily resultant of the pool table surface. In the cases of our trials, B rolls without sliding across T, so we allow note that μ_s is the active source of friction.

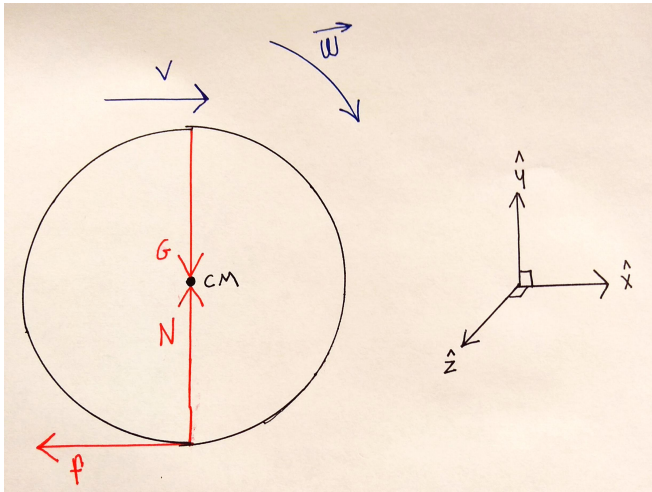

FIG. 1: Free-body diagram describing motion of a rigid sphere moving along a rigid flat surface. [4] Blue arrows indicate velocities, red arrows indicate forces, and black markings indicate background information, with B drawn on the left and Cartesian coordinate axes drawn on the right.

When engaged in 1-D motion parallel to T, it is known that B has a linear velocity v. Note that because B not only moves along T, but is also in rolling motion, B possesses angular velocity $\vec{\omega}$ as well. This angular velocity could, in theory, be used to calculate μ. However, angular interpretations of the motion of B are not advantageous to us. Our Cartesian coordinate system can be aligned to make the x-axis parallel both to v and to friction force f, as shown in Fig. 1. The other forces acting on B, which are gravitational force G and normal force N, can be set within the direction of the y-axis. Because of this, f, G, N, and v can be denoted as scalar quantities, as their directional components for their respective axes are equal to their magnitudes. By contrast, $\vec{\omega}$ has both x and y components, which needlessly makes calculations more complicated. Additionally, measuring the linear velocity of a pool ball in motion is simpler based on our apparatus, which will be described in the Section III. Finally, because B is a solid sphere of uniform density, the motion of B can effectively be analyzed by the center of mass CM of B, and because that point has an angular velocity of 0, angular velocity becomes an inept metric. [11]

Note that Assumption 7 requires that force F, which is exactly parallel to T, must be applied to B. Even if static friction prevented small components of F along the y- or z-axes from directly affecting linear motion, the nonzero incident angle (between the direction of F and the plane T) would cause spin factors that would have substantial effects on the motion of B. [2] This would also contribute to some semblance of bounciness of B, the minimization of which is necessary for Assumption 3. Consequently, our procedure will describe methods taken to ensure that F is in the appropriate direction.

We will now analyze the motion of B along the x-axis, which set as the direction of motion of B, as B has no net velocity or acceleration in the y-direction due to the cancellation of N and G. Note that in Fig. 1, the only force acting on B along the x-axis is f. Because no force counterbalances f, we know that in the case of $v \neq 0$ and $f \neq 0$, it holds that v will change over time t due to its acceleration a as a result of f. Note the existence of some initial velocity v_0 applied to B by the apparatus (described later) at time t_0. Basic kinematics tells us that

$$v_\tau = v_0 + a(t_0 - \tau) \tag{1}$$

for velocity v_τ at time τ. [5, 6] If we let τ be the exact time at which the motion of B ceases ($v_\tau = 0$), we derive

$$\frac{v_0}{t_0 - \tau} = a \ . \tag{2}$$

Generally speaking, we know B under non-sliding rolling motion experiences a friction force of

$$f = \mu_\mathrm{s} G \cos\theta \tag{3}$$

on a plane of incline θ from the xz-plane. [5, 6] Given our force laws $f = ma$ and $G = mg$, as well as that $\theta = 0$ for T (which is entirely on the xz-plane), we find

$$a = \mu_\mathrm{s} g \ . \tag{4}$$

Combining Eqs. (2) and (4) and simplifying yields

$$\mu_\mathrm{s} = \frac{v_0}{g(t_0 - \tau)} \ . \tag{5}$$

Note that the motion sensor and software we shall utilize (which will be described in the Section III) measures the position x of B with respect to t. The values for τ and t_0 can be identified by examining an $x(t)$ and identifying where the motion of B begins and ends. The value of v_0, which is not accurately measured by the motion sensor, is approximated by

$$v_0 \approx \frac{\Delta x}{\Delta t} \tag{6}$$

for minimum measurable change in time Δt that occurs once motion begins at t_0 and the change in position Δx that occurs over Δt. [5]

We let

$$\Delta t = t_1 - t_0 \text{ and } \Delta x = x_1 - x_0 \ , \tag{7}$$

where t_0 is time at which B is launched, t_1 is the first available time measurement after t_0, and x_0 and x_1 are the position measurements of B at t_0 and t_1, respectively. The value of g at Taylor Hall, the location at which this experiment takes place, is 9.801 m/s^2. [9, 12]

We now are able to calculate μ using only measurable or known quantities. Note that for the equipment we shall use (see Section III), we have position measurement uncertainties $\delta x = 0.001$ m and time measurement uncertainties of $\delta t = 0.001$ m. To find results from each trial, Eqs. (5), (7), and (6) combine to calculate each trial's friction coefficient

$$\mu_{\mathrm{s},i} = \frac{(x_{1_i} - x_{0_i})}{g\,(t_{1_i} - t_{0_i})\,(\tau_i - t_{0_i})} \tag{8}$$

at each trial i. Note that in Eq. (8), each previously defined variable is indexed by i but unchanged in meaning. The uncertainty of each $\mu_{\mathrm{s},i}$ measurement is taken as

$$\delta\mu = \left(\left(\frac{\partial\mu_i}{\partial x_{0_i}}\delta x_{0_i}\right)^2 + \left(\frac{\partial\mu_i}{\partial x_{1_i}}\delta x_{1_i}\right)^2 + \left(\frac{\partial\mu_i}{\partial t_{0_i}}\delta t_{0_i}\right)^2 + \left(\frac{\partial\mu_i}{\partial t_{1_i}}\delta t_{1_i}\right)^2 + \left(\frac{\partial\mu_i}{\partial \tau_i}\delta \tau_i\right)^2\right)^{\frac{1}{2}} \tag{9}$$

given values from Eq. (8). [3] Using these uncertainty values, we can use IGOR Pro to form a μ_i vs. i plot. Adding a linear fit to this plot allows us to find the weighted average with uncertainty of our μ_i data, which we will take to be μ. We also note the standard deviation

$$\sigma_\mu = \sqrt{\frac{1}{n-1}\sum_{i=1}^{n}(\mu - \mu_i)^2} \tag{10}$$

of μ. [10] To convey how substantial σ_μ is relative to μ, we will also show the error percentage of

$$P = \left|\frac{\sigma_\mu}{\mu}\right|(100\%) \tag{11}$$

relative to μ. Usually, only one of two theoretical friction coefficients act on a ball on a standard pool table: the kinetic friction coefficient μ_{k} (ball slides without rolling) or the static friction coefficient μ_{s} (ball rolls without sliding). For the cloth on a standard pool table to fit pool playing regulations, it must hold that $\mu_{\mathrm{s}} < 0.30$ in the case of rolling, or $\mu_{\mathrm{k}} < 0.03$ in the case of sliding. [6] We observe that B rolls without sliding when launched on T, so

$$\mu \leq 0.30 \tag{12}$$

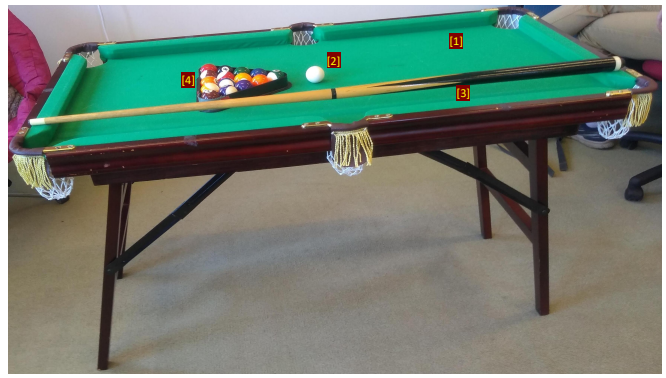

FIG. 2: The miniature pool table used for experimentation, with labels on 4 key areas. [1]: the pool table cloth surface T. [2]: the cue ball used for experimentation B. [3]: the pool cue stick with which a handful of pool games were played in order to get a physical sense of the apparatus. [4]: the pool balls utilized in the pool games referenced by [3].

if the cloth on T is to fit acceptable non-miniature pool table regulations. This upper bound may serve as a guidance, even if we know that there are differences between standard and miniature pool tables.

Note that our data collection on x and t is limited to the travel of B over a distance at or under to the length of T. Due to the high cushioning present on the sides of pool tables (i.e. on the edges of T), B colliding with said cushioning would result in a significant transfer of momentum at the moment of collision. [7] This momentum transfer would compromise our prior equations and result in inaccurate calculation of μ. Therefore, v_0 must be low enough to ensure that B can travel approximately the length of T (in order to collect maximum possible data) without colliding with the side of T.

III. PROCEDURE

For our experiment, we began with a miniature pool table, shown in Fig. 2. The surface of the pool table formed a rectangle, with dimensions measured to be (1.010 ± 0.005) m by (0.490 ± 0.005) m for the inner surface, plus (0.055 ± 0.005) m of cushioning on each side. The inner surface (without cushioning) was taken to be the plane T.

FIG. 3: The pool table after the levelling process. Observe the varying-sized stacks of paper towels under each leg of the pool table.

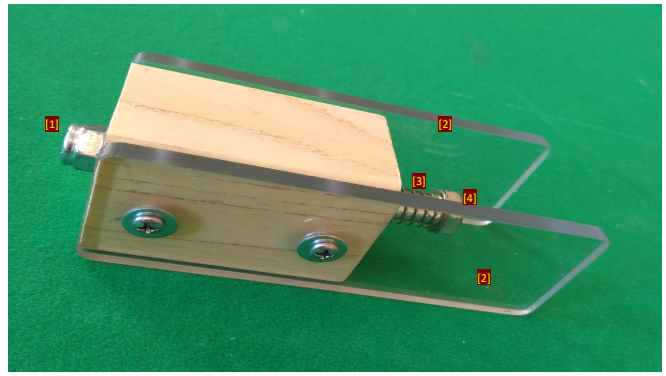

FIG. 4: Launching apparatus developed by Tim Siegenthaler. By pulling back bolt [1] and placing B in between side shields [2], spring [3] is compressed. By releasing bolt [1], the spring [3] decompresses, allowing bolt [4] to apply force F to B in a direction perpendicular to gravitational force G and parallel to T.

FIG. 5: PASCO motion sensor. The lens takes data points of the position and time of objects the sensor focuses on, then plots that data using PASCO Capstone software.

In order to gain a physical sense of the apparatus, a few games of pool were played using the miniature pool table, cue stick, and balls. During these games, it was consistently observed that most balls went towards one side of the pool table, with 2 adjacent pockets containing the vast majority of balls by the end of each game. Upon observing this phenomenon, we decided to conduct tests to determine whether or not the table was level. Upon discovering that the table was not level, a considerable amount of time was spent placing a varied number of paper towels under each leg of the pool table until the pool table was measured to be level throughout its surface. Making the pool table level ensured that gravitational acceleration and frictional acceleration were orthogonal when B was launched across the T, which was crucial to justify the $\theta = 0$ substitution for Eq. (3). This levelling process therefore validates Assumption 6. The levelled pool table is shown in Fig. 3.

Our goal was to launch B across T and analyze how the position x of B changed over time t. Assumptions 6 and 7 required us to give B an initial velocity v_0 exactly parallel to the perfectly flat (orthogonal to gravitational force) plane T. Therefore, a piece of equipment needed to be constructed that applied a perfectly horizontal point force to B that allowed the position of B to be constrained entirely to the x-axis. Additionally, as discussed in the Section II of this report, v_0 had to be small enough to ensure that B did not have a collision with the edges of T. In order to design the equipment to fit our specifications, the mass m of B had to be measured, and the radius r of B had to be calculated. Using a standard electronic scientific scale, we measured $m = (51.27 \pm 0.01)$ g. Via indirect measurement of circumference $C = 2\pi r$ (we were unaware of calipers at the time), we calculated $r = (0.124 \pm 0.001)$ cm. The resulting m and r values, along with the desired equipment specifications, were sent to machinist Tim Siegenthaler. Siegenthaler constructed and supplied us with a spring-based launching device to apply the appropriate point force F to launch B directly along T such that B did not collide with the edge of T. This launcher is shown in Fig. 4.

To measure x and t values, a motion sensor with PASCO Capstone software, shown in Fig. 5, was utilized. The motion sensor lens created a plane perpendicular to the direction of v_0. For each trial, the motion sensor and corresponding software generated scatter plots of x versus t, similar to the one that will be shown in the Section IV of this report, for the motion of B induced by applied force F. Data was extracted from these plots and used to calculate μ_i.

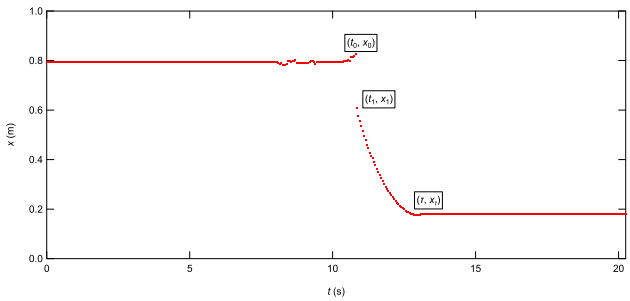

FIG. 6: Scatter plot of x versus t for the motion of B. Note that the approximate locations of t_0, t_1, τ, x_0, and x_1 are marked, and that we let x_τ be the position of B at $t = \tau$. The point (t_0, x_0) is the measurement nearest to the start of the motion of B. The point (t_1, x_1) is the first measurement taken after (t_0, x_0). The point (τ, x_τ) is the measurement at which the velocity of B initially hits an approximate value of 0, as determined by the cessation of B's motion with respect to its initial direction.

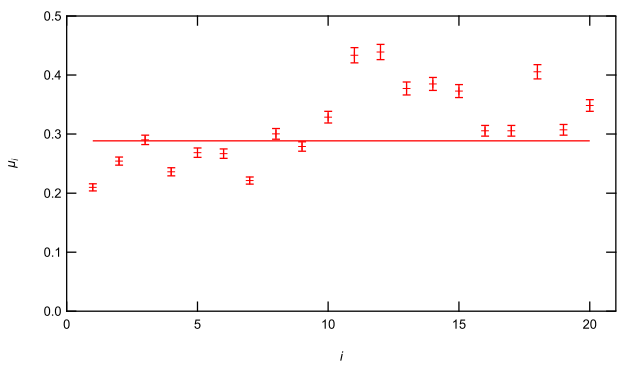

FIG. 7: Scatter plot of μ_i versus t for the μ_i values calculated in Appendix A. Weighted (by $\delta\mu_i$) average from zero-slope linear fit was calculated to be $\mu = 0.288 \pm 0.002$.

IV. RESULTS & ANALYSIS

20 trials were able to be used for our data analysis. For each trial, scatter plots of x versus t were generated as B moved directly towards the motion sensor lens. The plot for an example run is shown in Fig. 6. The relevant data points $t_0,\ t_1,\ \tau,\ x_0$, and x_1 were extracted from these graphs.

By using the data collected from a series of such scatter plots for each trial i, calculations were made using Eq. (8) to calculate each μ_i value and using Eq. (9) to calculate each $\delta\mu_i$ value. Recall for this purpose that all position measurements had uncertainties of 0.001 m and that all time measurements had an uncertainties of 0.001 s. The μ_i values by run are shown Fig. 7.

The weighted linear fit from Fig. 7 yielded a weighted average of $\mu = 0.288 \pm 0.002$, which we take as our final value. The value was chosen to have 3 digits after the decimal point, as that was the precision of our instrumentation. The standard deviation of μ, found via Eq. (10), was found to be $\sigma_\mu = 0.074$. Note that by Eq. (11), it is calculated that σ_μ is a relative percent error $P = 25.6$ % of μ. Because $\mu < 0.30$, the cloth used on T is concluded to be within standard pool table cloth regulations under the parameters described in Eq. (12). However, the validity of this test for miniature pool tables is still unknown.

Although the relative percent error for μ is not remarkably high, it is certainly considerable. Most likely, this error can be contributed to some flaws in our assumptions (described at the beginning of the Section II of this report). For example, Assumption 4, which states that the friction coefficient of B is negligible, may be false, which could have affected the spin motion of B and caused motion that deviates from our equations of motion. [6] Similarly, Assumption 3, which states that T is perfectly rigid, may have made our equations of motion overly simplified for our system, which would affect our μ calculation. [4] There might also have been some issue with our apparatus that would cause B to take a non-straight path, or a straight path that isn't exactly perpendicular to the motion sensor. However, our error is fairly low considering the number of assumptions and simplifications made to model this system, so the range obtained with our μ value should be taken as approximately accurate. We also observe that although our standard deviation percent error is high, our actual error value on μ seems reasonably low, which is likely due to the high precision of our instrumentation.

V. CONCLUSION

In order to calculate the friction coefficient μ acting on miniature pool table surface plane T, a pool ball B was launched along T in motion parallel to the plane of T. The position x and time t were measured and recorded by PASCO Capstone motion sensing technology and software, then put into x versus t scatter plots. Each trial i of our experiment involved generating one such scatter plot, then extracting relevant data from it in order to calculate that trial's friction coefficient μ_i and uncertainty $\delta\mu_i$ using constant $g = 9.801$ m/s^2 and Eqs. (8) and (9). The μ_i plots corresponding to the extracted data are shown in Fig. 7. Using a weighted linear fit, the average value with error was calculated to be $\mu = 0.288 \pm 0.002$. Using Eq. (10), the standard deviation was found to be $\sigma_\mu = 0.074$. Using Eq. (11), the relative percent error of the standard deviation $P = 25.6\%$ was calculated. By Eq. (12), it is concluded that our calculated μ value would qualify T as having pool table cloth satisfying standard pool table regulations.

There were several constraints that affected this ex-

periment, including limited research time, non-standard pool materials, and motion-sensing software that only measured time increments as low as 0.05 s. To accommodate for these constraints, many assumptions and approximations had to be made to simplify our system as much as possible. As a result, our calculated value for μ may be inaccurate, particularly given that its relative percent error of standard deviation is over 25%. In order to find more accurate values for μ, either on this pool table or on others, more information regarding specific constants of the corresponding pool table would need either to be provided or to be calculated within an extended research project. More precise apparatuses could also be constructed to ensure that B follows the requisite motion, which was only approximately the case within our experiment. Another helpful change to this experiment would be the utilization of a high-speed motion camera rather than a standard motion sensor.

VI. ACKNOWLEDGMENT

Thanks go to Dr. Niklas Manz for his assistance and suggestions during the experimentation process. Thanks go to the Physics Department at the College of Wooster for providing the miniature pool system used in this experiment. Thanks go to Timothy Siegenthaler for developing the launching apparatus necessary to generate the appropriate motion of the pool ball.

[1] Billiard Congress of America (BCA). About the Industry. https://bca-pool.com/page/39. Accessed on 30 March 2022.

[2] R. Cross. Bounce of a spinning ball near normal incidence. *AMERICAN JOURNAL OF PHYSICS*, 73(10):914–920, OCT 2005.

[3] Department of Physics, The College of Wooster, Wooster, OH. *Physics Junior Independent Study Lab Manual*, 2022.

[4] J. Hierrezuelo and C. Carnero. Sliding and Rolling: The Physics of a Moving Ball. *Physics Education*, 30(3):177 – 182, 1995.

[5] S. J. Ling, J. Sanny, and W. Moebs. *University Physics: Volume 1*. Rice University, Houston, TX, 2017. ISBN: 978-1-947172-20-3.

[6] W. C. Marlow. *The Physics of Pocket Billiards*. MAST, Palm Beach Gardens, Florida, 1995. ISBN: 0964537001.

[7] S. Mathavan, M. R. Jackson, and R. M. Parkin. A theoretical analysis of billiard ball dynamics under cushion impacts. *PROCEEDINGS OF THE INSTITUTION OF MECHANICAL ENGINEERS PART C-JOURNAL OF MECHANICAL ENGINEERING SCIENCE*, 224(C9):1863–1873, 2010.

[8] K. Ragoo, V. Sirjoosingh, S. Sahadeo, B. V. Chowdary, and C. Maharaj. Design and development of a pool and billiards assistive device for the physically challenged. *Disability & Rehabilitation: Assistive Technology*, 14(6):628 – 634, 2019.

[9] N. N. G. Survey. Surface Gravity Prediction. https://geodesy.noaa.gov/cgi-bin/grav_pdx.prl. Accessed on 27 March 2022.

[10] J. R. Taylor. *An Introduction to Error Analysis: The Study of Uncertainties in Physical Measurements*. University Science Books, Sausalito, California, 1997. ISBN: 9780935702750.

[11] J. R. Taylor. *Classical Mechanics*. University Science Books, Sausalito, California, 2005. ISBN: 189138922X, 9781891389221.

[12] The College of Wooster Physics Department. OSAPS/AAPT/SPS 2019: Frontiers in Nonlinear Science. https://physics.wooster.edu/osaps-aapt-sps2019/, 2019. Accessed on 27 March 2022.

Appendix A: Data Values

This appendix presents all data utilized from each of our 20 runs for the purposes of verifying our calculations if necessary. The necessary data is shown in Table I.

TABLE I: The data obtained via analysis of the graphs of our 20 runs, as well as μ_i values calculated by Eq. (8) and $\delta\mu_i$ values calculated by Eq. (9) at each run using said data and constant $g = 9.801\,\mathrm{m/s^2}$.

i	t_{0_i} (s)	t_{1_i} (s)	τ_i (s)	x_{0_i} (m)	x_{1_i} (m)	μ_i	$\delta\mu_i$
1	10.800	10.850	12.900	0.825	0.609	0.210	0.006
2	11.000	11.050	12.950	0.828	0.585	0.254	0.007
3	12.250	12.300	14.100	0.838	0.575	0.290	0.008
4	12.000	12.050	14.100	0.844	0.601	0.236	0.007
5	12.900	12.950	14.250	0.841	0.591	0.269	0.008
6	12.200	12.250	14.250	0.841	0.573	0.267	0.008
7	9.750	9.800	12.000	0.836	0.592	0.221	0.006
8	9.800	9.850	11.600	0.834	0.569	0.300	0.009
9	12.000	12.050	14.150	0.851	0.557	0.279	0.008
10	11.100	11.150	13.100	0.846	0.524	0.329	0.010
11	11.600	11.650	13.200	0.859	0.519	0.434	0.013
12	15.500	15.550	17.150	0.866	0.511	0.439	0.013
13	12.100	12.150	13.950	0.855	0.513	0.377	0.011
14	10.000	10.050	11.850	0.869	0.520	0.385	0.011
15	10.950	11.000	12.800	0.860	0.522	0.373	0.011
16	11.250	11.300	13.300	0.857	0.550	0.306	0.009
17	11.050	11.100	13.200	0.857	0.535	0.306	0.009
18	12.400	12.450	14.050	0.857	0.529	0.406	0.012
19	12.150	12.200	14.150	0.849	0.548	0.307	0.009
20	10.550	10.600	12.400	0.872	0.556	0.349	0.010